scientific reports

Check for updates

OPEN

ACPA prevents lung fibroblast-to-CAF transformation by reprogramming the tumor microenvironment through NSCLC-derived exosomes

Özge Boyacıoğlu[1], Berfin Deniz Kalali[1,2], Tuba Reçber[3], Dilek Gelen-Gungor[4,5], Emirhan Nemutlu[3], İpek Eroğlu[2,5], Nedret Kılıç[1] & Petek Korkusuz[2,6,7]✉

Non-small cell lung cancer (NSCLC) accounts for most lung cancer cases. Current treatments often cause systemic side effects or lead to drug resistance, prompting the development of new therapies targeting tumors and related cells simultaneously. Cancer-associated fibroblasts (CAFs) are crucial stromal cells within the tumor microenvironment (TME), making them potential targets for therapy. Previously, we found that the CB1 receptor agonist ACPA has anti-tumor effects on NSCLC, inhibiting pathways such as Akt/PI3K, JNK, glycolysis, the citric acid cycle, and the urea cycle both in vitro and in vivo. We hypothesize that ACPA could enhance therapy by inhibiting the transformation of lung fibroblasts into CAFs via exosomes. Control and ACPA-treated NSCLC cell exosomes exhibited similar size, PDI, ZP, and high expression of CD9, CD63, and CD81. ACPA-treated exosomes showed reduced levels of miR-21 and miR-23. These exosomes decreased fibroblast viability within 12 h by disrupting pentose phosphate, lipid, and amino acid metabolism, and by lowering PDPN, α-SMA, and FAP expressions. This research highlights ACPA as a promising chemotherapeutic agent, capable of improving NSCLC treatment and reprogramming the TME with more targeted therapies.

Keywords Non-small cell lung cancer, Exosomes, Cancer-associated fibroblasts (CAFs), Arachidonylcyclopropylamide (ACPA), Tumor microenvironment (TME)

Lung cancer (LC) is the most frequently diagnosed malignancy at a late stage, accounting for 12.4% of all cancer cases[1]. The exceptionally high global mortality rate results directly from the fact that only 15% of patients are diagnosed early, while approximately 70% are identified at a late metastatic stage[2]. Non-small cell lung cancer (NSCLC) makes up 87% of all LC cases[3]. In cases of advanced-stage NSCLC where surgery is considered unsuitable, management strategies[4] often encounter significant limitations such as systemic adverse effects, autoimmune-like reactions, or immune-related toxicity[5,6]. This underscores the need for the development of novel therapeutics that effectively target the tumor microenvironment (TME)[7,8], with a tolerable side effect profile at lower therapeutic concentrations.

Cancer-associated fibroblasts (CAFs) are widely distributed stromal cells within the solid TME[9], stimulating cancer cell proliferation, metastasis and angiogenesis via secretomes (Interleukin-6/-8/-11 (IL-6/-8/-11)), chemokines and transforming growth factor beta (TGF-β)[10], including NSCLC[11,12]. Unlike healthy fibroblasts, CAFs, highly express alpha smooth muscle actin (α-SMA), phosphorylated Smad2 (pSmad2), fibroblast activation protein (FAP) and podoplanin (PDPN)[13], contributing to regulate immunosuppression, inducing cancer proliferation, invasion and migration, remodeling the extracellular matrix, promoting angiogenesis[11,14]

[1]Department of Medical Biochemistry, Faculty of Medicine, Atılım University, 06830 Ankara, Turkey. [2]Department of Bioengineering, Graduate School of Science and Engineering, Hacettepe University, 06800 Ankara, Turkey. [3]Department of Analytical Chemistry, Faculty of Pharmacy, Hacettepe University, 06100 Sıhhiye, Ankara, Turkey. [4]Department of Forensic Sciences, Turkish National Police Academy, 06834 Ankara, Turkey. [5]Department of Basic Pharmaceutical Sciences, Faculty of Pharmacy, Hacettepe University, 06100 Ankara, Turkey. [6]Department of Histology and Embryology, Faculty of Medicine, Hacettepe University, 06100 Sıhhiye, Ankara, Turkey. [7]METU MEMS Center, 06530 Ankara, Turkey. ✉email: petek@hacettepe.edu.tr

and inhibiting apoptosis by PI3K/Akt/mTOR and Hedgehog activation[15]. Moreover, the interaction of CAFs with cancer/cancer stem cells induces tumor progression by regulating cell plasticity and ensures the preservation of the cancer stem cell pool[11], thereby develops resistance to chemotherapeutic agents[16]. Therefore, targeting CAFs is crucial for suppressing progression within the TME.

Cannabinoids (CB) reduce cell proliferation and metastasis[17] and induce apoptosis[7] in NSCLC via CB1/2 receptors. We further reported a dose- and time-dependent anti-proliferative and apoptotic therapeutic window for synthetic CB1 receptor agonist Arachidonylcyclopropylamide (ACPA) on NSCLC via Akt/PI3K, JNK, glycolysis, citric acid cycle and urea cycle pathways in vitro and in vivo[18–20], as well as other CB agonists on solid cancers including endometrial cancer[21] and osteosarcoma[22]. However, targeting tumor cells alone may not be sufficient for the translational therapeutic efficacy of cannabinoid derivatives. CAFs, which facilitate the spread of cancer cells in the TME, are reported to be among the critical treatment targets of NSCLC[11]. As a potential TME regulator, ACPA can strengthen the therapeutic potential by reducing the tumor-inducing behavior of CAFs.

NSCLC exosomes promote tumor development by inducing the transformation of healthy lung epithelial cells and fibroblasts within the TME[23]. Cannabidiol-containing exosomes diminished cell viability, led to cell cycle arrest at G0/G1 phase and triggered apoptosis in hepatocellular carcinoma[24]. Co-application of cannabidiol and temozolomide (TMZ) reduced pro-oncogenic miR-21 and increased anti-oncogenic miR-126 in glioblastoma exosomes[25]. Preserving healthy fibroblast populations may be a therapeutic target to prevent peritumoral invasion. Therefore, we aimed to protect the healthy fibroblast population in the tumor stroma and prevent their transformation into CAFs by examining the effect and mechanism of action of ACPA on the release profile of NSCLC cell-derived exosomes and the potency of transformation of healthy lung fibroblasts (HLFs) into CAFs for the first time.

Results

NSCLC exosomes exhibited a homogeneous particle size range, optimum polydispersity index and zeta potential values

Control and ACPA-treated NSCLC cell exosomes exhibited protein concentrations of 312.44 and 460.96 µg/ml, respectively, by BCA. Their particle size (PS), polydispersity index (PDI) and zeta potential (ZP) were 250.97 ± 85.45 and 317.33 ± 277.34 nm; 0.50 ± 0.23 and 0.56 ± 0.20; and -11.66 ± 5.83 and -23.13 ± 2.06 mV, respectively, by Zeta Sizer. Control exosomes presented CD9, CD63 and CD81 labelling as 96.93%, 98.35% and 77.33% by flow cytometry (FCM), respectively. ACPA-treated NSCLC cell exosomes labelled with CD9, CD63 and CD81 were 95.75%, 95.86% and 70.16%, respectively (Fig. 1c). Quantitative TEM revealed the mean diameter of control A549 cell exosomes as 147 ± 39 nm; and ACPA-treated ones as 132 ± 46 nm (Fig. 1d-f). Control NSCLC cell exosomes presented a mean PS and concentration of 150.0 ± 47.3 nm and $9.69 \times 10^9 \pm 1.50 \times 10^8$ particles/ml (Fig. 1g, h) by nanoparticle tracking analysis (NTA). ACPA-treated NSCLC cell exosomes exhibited a mean PS and concentration of 268.3 ± 69.8 nm and $7.21 \times 10^{10} \pm 2.94 \times 10^{10}$ particles/ml (Fig. 1i, j) by NTA.

ACPA suppresses oncogenic miRNAs in NSCLC exosomes and reduces fibroblast viability

IC50 ACPA significantly reduced miR-21 ($p = 0.007$) and miR-23a ($p = 0.041$) expression in NSCLC exosomes compared to control (Fig. 2a). ACPA-applied NSCLC exosomes at 100 µg/ml significantly decreased HLF viability on day 1 ($p < 0.05$), whereas 10 µg/ml of exosomes increased fibroblast viability compared to control (Fig. 2b). Similarly, ACPA-applied NSCLC exosomes at 10 and 50 µg/ml diminished fibroblast viability compared to control exosomes at 100 µg/ml, control exo-free medium and A549:LL24 co-culture groups on day 1 by RTCA ($p < 0.05$, Fig. 2e). ACPA-applied NSCLC exosomes at 10 and 50 µg/ml did not diminish cell viability on days 2–3 ($p < 0.05$, Fig. 2c-d). ACPA-applied NSCLC exosomes at 10 µg/ml dose reduced cell viability compared to A549:LL24 co-culture groups on days 2 and 3 ($p < 0.05$); conversely, it lost its anti-proliferative activity on HLFs compared to controls ($p > 0.05$, Fig. 2e). IC50 of control and ACPA-applied NSCLC exosomes were calculated as 106.8 ($R^2 = 1$; Fig. 2f) and 45.1 ($R^2 = 1$; Fig. 2g) µg/ml, respectively following 12 h of application. Co-culture of A549:HLFs with 5:1 ratio exhibited a superior anti-proliferative effect on HLFs when compared to 1:1 and 1:5 A549:LL24 co-culture groups (Fig. 2h) and the treatment responses of 50% and 80% of fibroblasts were at 25 and 56 h following the initiation of co-culture model (Fig. 2i). The treatment responses of 50% of the fibroblasts reached 28 and 38 h following the initiation of 1:1 and 1:5 co-culture models (Fig. 2i).

Treatment of HLFs with ACPA-administered NSCLC cell-derived exosomes (50 µg/ml) resulted in a marked reduction in mean PDPN immunolabeling, which decreased to 62.36% on day 1 ($p = 0.0164$, Fig. 3a, d). In contrast, fibroblasts cultured in control medium exhibited 73.04% PDPN labeling. Mean FAP expressions were 96.50 and 82.42% in control exosomes-treated and negative control fibroblasts, and 94.28% in ACPA-treated exosome-applied fibroblasts ($p = 0.0208$, Fig. 3b, e). Mean α-SMA labeling was 87.93% and 89.43% in fibroblasts treated with control exosomes and exosome-depleted medium, respectively, whereas ACPA-treated exosomes significantly reduced α-SMA expression to 44.76% ($p = 0.0013$, Fig. 3c, f).

HLFs treated with ACPA-administered NSCLC cell-derived exosomes at 10, 50 and 100 µg/ml exhibited increased IL-6 and IL-8 secretion on days 1–3 compared to control medium ($p < 0.05$, Fig. 3g, h). Control NSCLC exosomes at 100 µg/ml showed a reduction in IL-6 release from the fibroblasts on day 1 compared to ACPA-administered NSCLC exosomes or control medium (Fig. 3g). ACPA-administered NSCLC cell-derived exosomes at 50 and 100 µg/ml increased IL-6 release in HLFs on days 2–3 ($p < 0.05$), while they decreased IL-8 release like the control (Fig. 3h).

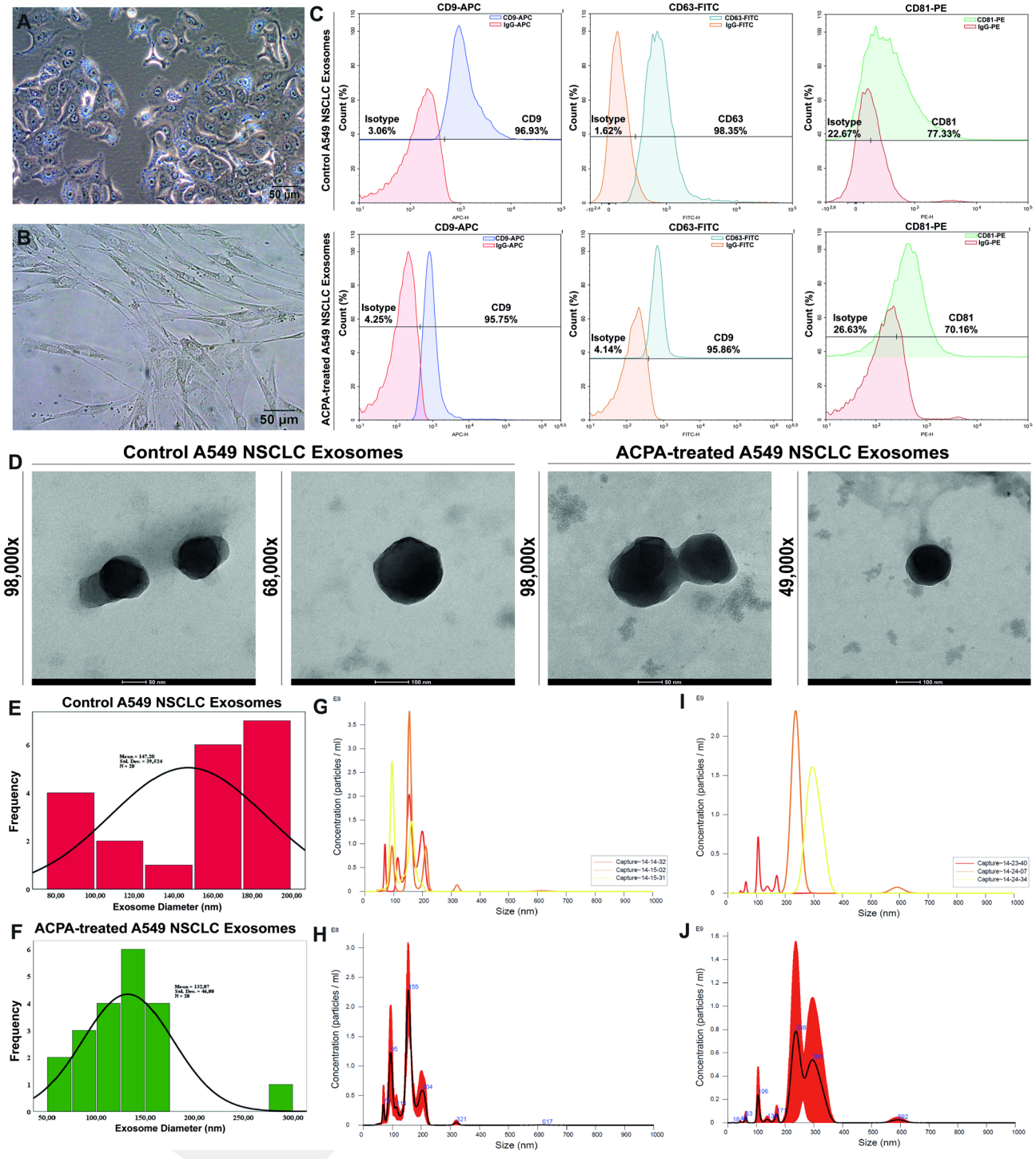
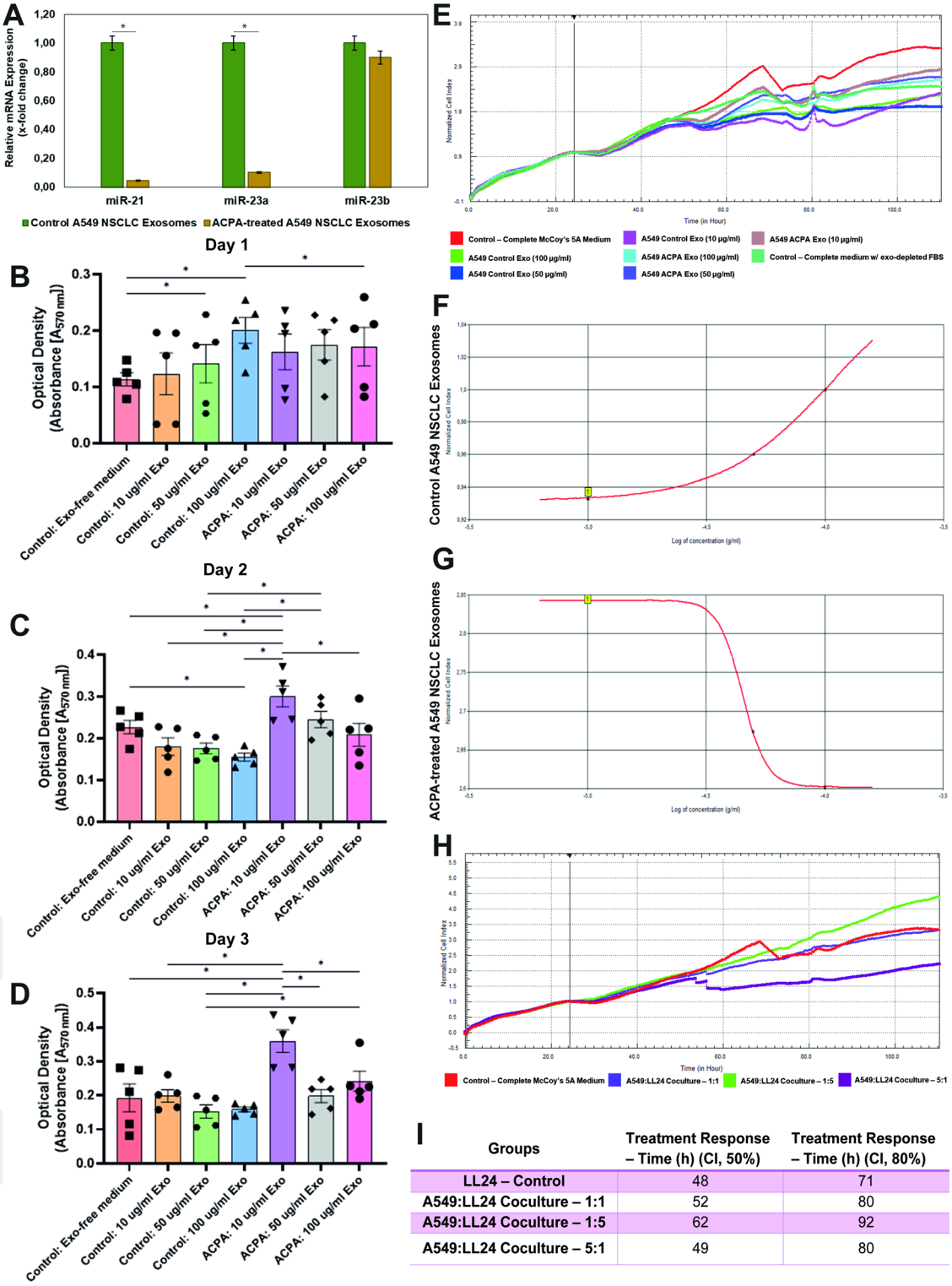


Fig. 1. Control and IC50 ACPA-applied NSCLC cell exosomes were successfully characterized. **a**, **b** Micrographs representing phase-contrast (PC, scale bar, 50 µm) view of (**a**) A549 NSCLC and (**b**) LL24 healthy human lung fibroblasts, 400x. (**c**) Flow cytometric analysis of tetraspanin CD9, CD63 and CD81 markers in control and ACPA-applied A549 cell exosomes. Fluorescence (CD9-APC, CD63-FITC and CD81-PE) on the x-axis vs. number of events (Count (%)) on the y-axis ($n = 3$). **d–f** TEM analysis. (**d**) TEM images and (**e**, **f**) size distribution diameters from TEM images of control and ACPA-applied A549 cell exosomes ($n = 20$). **g–j** Representative NTA of (**g**, **h**) control and (**i**, **j**) ACPA-applied A549 cell exosomes under 100x dilutions. Graphs ***g*** and ***i*** depict the finite track length adjustment (FTLA) size per concentration as triplicates and graphs ***h*** and ***j*** depict the average FTLA size per concentration.



I

Groups	Treatment Response – Time (h) (CI, 50%)	Treatment Response – Time (h) (CI, 80%)
LL24 – Control	48	71
A549:LL24 Coculture – 1:1	52	80
A549:LL24 Coculture – 1:5	62	92
A549:LL24 Coculture – 5:1	49	80

Fig. 2. ACPA-applied NSCLC cell exosomes at a lower dose diminish LL24 HLFs compared to control within 12 h. (**a**) qRT-PCR analysis for relative miRNA fold change values of miR-21, miR-23a and miR-23b relative to U6 gene ($n = 4$). **b–d** Proliferation indices of LL24 HLFs following the application of control or ACPA-applied A549 NSCLC cell exosomes at doses of 10, 50 and 100 µg/ml for (**b**) 1, (**c**) 2 or (**d**) 3 days by MTT assay in mean ± SEM ($n = 5$, $^*p < 0.05$ by one-way analysis of variance (ANOVA) and post-hoc Duncan's test). All proliferation data are presented in absorbance (A570 nm). **e–h** Real-time normalized proliferation indices of (**e**) control or ACPA-applied A549 NSCLC cell exosome-administered HLFs presented with control and exosomes at doses of 10, 50 and 100 µg/ml along with the IC50 graphs of (**f**) control and (**g**) ACPA-applied A549 NSCLC cell exosomes for 4 days ($n = 3$ for exosome-applied groups and $n = 6$ for controls) and (**h**) LL24 fibroblasts following co-culture with A549 cells at ratio of 1:1, 1:5 or 5:1 ($n = 6$). (**i**) Treatment response time points of LL24 fibroblasts following co-culture with A549 cells when cell index (CI) is at 50 or 80%.

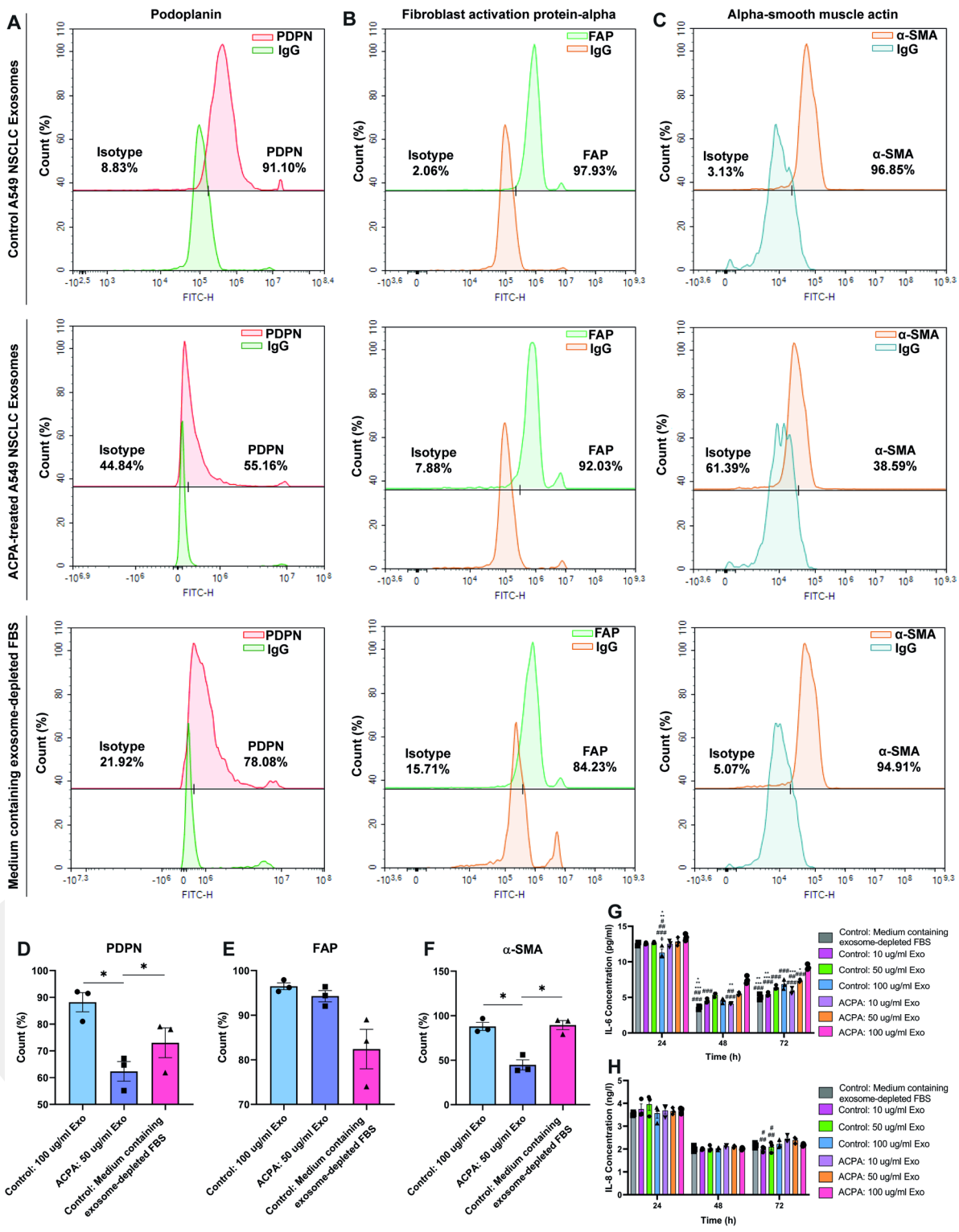


Fig. 3. ACPA-applied NSCLC cell exosomes at a lower dose inhibited PDPN, FAP and α-SMA expressions in HLFs compared to control. Representative univariate histograms (**a–c**) and bar graphs (**d–f**) of FCM depicting the expressions of (**a**, **d**) PDPN, (**b**, **e**) FAP and (**c**, **f**) α-SMA in LL24 fibroblasts following control or ACPA-applied A549 NSCLC cell exosomes at doses of 100–50 µg/ml, respectively ($n = 3$). **g-h** Secretome profile of LL24 fibroblasts including (**g**) IL-6 and (**h**) IL-8 on days 1, 2 and 3 following the application of control or ACPA-applied A549 NSCLC cell exosomes at doses of 10, 50 and 100 µg/ml by ELISA. ($n = 3$, $^*p < 0.05$ by one-way analysis of variance (ANOVA) and post-hoc Duncan's test).

ACPA-applied NSCLC cell exosomes diminish fibroblast viability through carbohydrate, lipid and amino acid metabolic pathways

PCA graphs of the LL24 fibroblast metabolites following ACPA-applied exosome, control exosome or control medium evidently present significant differences (Fig. 4a, b). ACPA-applied NSCLC cell exosomes at 50 µg/ml inhibited fibroblast growth through suppressing erythrose 4-phosphate, glucose and glucuronic acid levels and increasing mannitol level related to carbohydrate metabolism (Fig. 4c, d, e). ACPA-applied NSCLC exosomes also diminished cholesterol, alanine, glycine, isoleucine and norleucine levels in fibroblasts but promoted malonic acid level (Fig. 4c, d, f, g). Control NSCLC exosomes decreased flavin adenine dinucleotide (FAD) level in fibroblasts (Fig. 4c, d, h). ACPA-applied NSCLC exosomes did not alter the levels of glyceraldehyde, maltose, maltitol, gluconic acid, gluconic acid lactone, N-acetyl-D-glucosamine and glucosaminic acid related to carbohydrate metabolism (Fig. 4e); arachidic acid, heptadecanoic acid, glycerol 1-phosphate, beta-glycerolphosphate regarding the lipid metabolism (Fig. 4f); glutamic acid and hypotaurine related to amino acid metabolism (Fig. 4g); guanosine-5'-monophosphate regarding nucleotide metabolism (Fig. 4h) and citric acid (crebs cycle), glycolic acid (cori cycle) and lactic acid (glyoxylate pathway) (Figs. 4i and 5).

Discussion

In this study, we demonstrated that effectively isolated ACPA-treated NSCLC exosomes expressed high levels of CD9, CD63, and CD81. ACPA suppressed oncogenic miR-21 and miR-23 in NSCLC cell exosomes. ACPA-treated NSCLC exosomes decreased HLF viability within the first 12 h, reduced expressions of PDPN, FAP, and α-SMA, and ultimately lowered the transformation potential into CAFs by inhibiting the pentose phosphate pathway and lipid and amino acid metabolism. ACPA-administered NSCLC exosomes did not alter IL-6 and IL-8 secretion profiles of HLFs between 24 and 72 h. Our group has previously shown the dose- and time-dependent anti-tumor effect of ACPA on NSCLC in vitro and in vivo (Turkish Patent and Trademark Office App.No: TR2019/12451; Patent Cooperation Treaty App.No: PCT/TR2020/050618)[18–20,26]. Building on this, HLFs treated with NSCLC exosomes underwent transformation and highly expressed CAF markers. Conversely, ACPA suppressed the capacity of HLFs to transform into CAFs at a notably low dose (1 pM), in this study.

IC50 ACPA-treated NSCLC exosomes were effectively isolated by ultracentifugation. Control and ACPA-treated NSCLC cell exosomes exhibited PS as 250.967 ± 85.451 and 317.333 ± 277.338 nm. The PDI values were 0.498 ± 0.232 and 0.563 ± 0.205, and the ZP values were − 11.663 ± 5.830 and − 23.133 ± 2.060 mV, respectively. As ultracentrifugation is regarded as the gold standard method for exosome isolation[27], it was employed in this study to obtain large-scale exosomes. NSCLC exosomes had a PDI value of 0.4–0.5, an average PS of 110–140 nm, and a ZP of -10 mV[28]. When Docetaxel was loaded into NSCLC exosomes, PDI, PS, and ZP values varied as 0.5–0.6, 120–160 nm and 21.1 mV, respectively. The PDI values of control NSCLC exosomes in the present study are consistent with the characterization data reported for the control NSCLC exosomes in the literature. Herein, ACPA was not loaded into NSCLC cell exosomes and applied directly to NSCLC cells. However, its exposure to parental NSCLC cells might have modulated intracellular pathways regarding vesicle formation and secretion, leading to alterations in exosome characteristics. Alternatively, the tumor cells are known to metabolize anti-cancer drugs through exosome release[29]. Once ACPA is applied to NSCLC cells, it could either bind to the CB1 receptor or be internalized through endocytosis and may subsequently be exported within exosomes regarding cell-based loading[30] and released into the extracellular space via exocytosis. The difference in PS between the control and ACPA groups could be attributed to ACPA being encapsulated in NSCLC cell exosomes. Control and ACPA-applied A549 cell exosomes expressed CD9, CD63, and CD81 markers as 96.93%, 98.35% and 77.33%; and 95.75%, 95.86% and 70.16%, respectively, in our research. Plasma-derived exosomes exhibited average CD9, CD63, and CD81 expression levels of 35%, 7% and 15%, respectively, by FCM in NSCLC patient plasma samples[31]. In this study, NSCLC exosomes displayed higher expression of CD9, CD63 and CD81 by FCM compared to the previous research, which ensures the purity of the population. High CD9, CD63, CD81, Hsp90 and/or Tsg101 protein levels were also detected in A549 NSCLC cell exosomes by Western blot[32,33]. FCM allows direct membrane labeling for triple-positive exosome verification, while Western blot has a total CD9, CD63, and CD81 labeling capability in cell/exosome lysates. Whole characterization data confirm the successful isolation of a highly pure exosome population that ensure the reliability of subsequent experiments.

Herein, IC50 ACPA reduces miR-21 and miR-23a levels by 20- and 10-fold and miR-23b level by 1.1-fold in NSCLC exosomes compared to control, which are known to be elevated in NSCLC and their exosomes compared to healthy lung cells, making them potential prognostic markers[34]. MiR-23a level in hypoxic LC cells increased 5-fold compared to normoxic cells[35]. Co-administration of cannabidiol at 1–5 µM and TMZ diminished the miR-21 expression 5- and 1.82-fold and promoted anti-oncogenic miR-126 expression 2.5- and 6-fold in LN18 and CRL-2611 glioblastoma cell-derived exosomes[25] which were lower than that of lower IC50 ACPA. These original findings indicate that ACPA is a potent suppressor of the oncogenic properties of miR-21 and miR-23 in NSCLC cell exosomes, which might improve the prognosis of NSCLC.

We demonstrated the effectiveness of ACPA-treated and control NSCLC exosomes at 50 and 100 µg/ml, respectively, using IC50 in HLFs within the first 12 h with the MTT assay and RTCA. Our experimental approach was systematic, starting with determining the optimal therapeutic window via MTT and pinpointing the specific dose and timing for maximum anti-fibrotic effect through real-time proliferation analysis (RTCA), which served as initial viability assessments. We also confirmed that MTT and RTCA results were consistent, showing the best therapeutic response at 12 h- a key time for capturing metabolic changes before full cellular phenotype shifts. Doses of 50 and 100 µg/ml for ACPA-treated and control exosomes were chosen based on RTCA curves and min-max cell indices. The anti-proliferative and CAF activation-inhibiting effects of ACPA-exosomes were strongest within the first 12–24 h, likely involving rapid cargo delivery that triggers cellular shock responses, temporarily suppressing activation pathways. Lower doses may cause mild stress, showing a biphasic, hormetic-like response[36]. Within this context, low concentrations of ACPA-treated exosomes did not

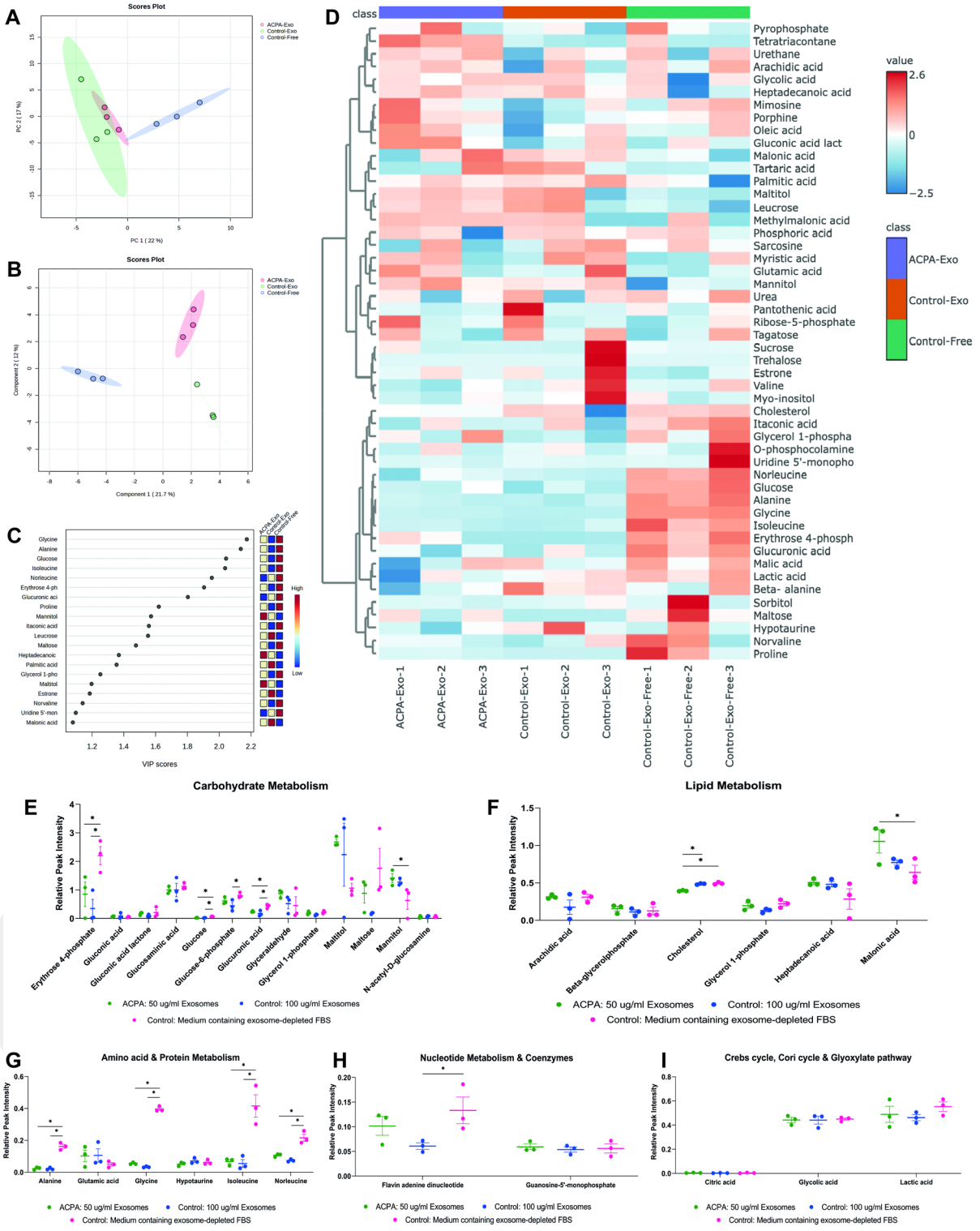


Fig. 4. ACPA-applied NSCLC cell exosomes reduce fibroblast growth via carbohydrate, lipid and amino acid metabolic pathways. (**a–b**) PCA plots, (**c**) VIP scores, (**d**) heat maps and (**e–i**) mean-standard deviation graphs of metabolites of LL24 fibroblasts following treatment of ACPA-applied and control NSCLC cell exosomes and control medium containing exosome-depleted FBS ($n = 3$, $^*p < 0.05$ by one-way analysis of variance (ANOVA) and post-hoc Duncan's test).

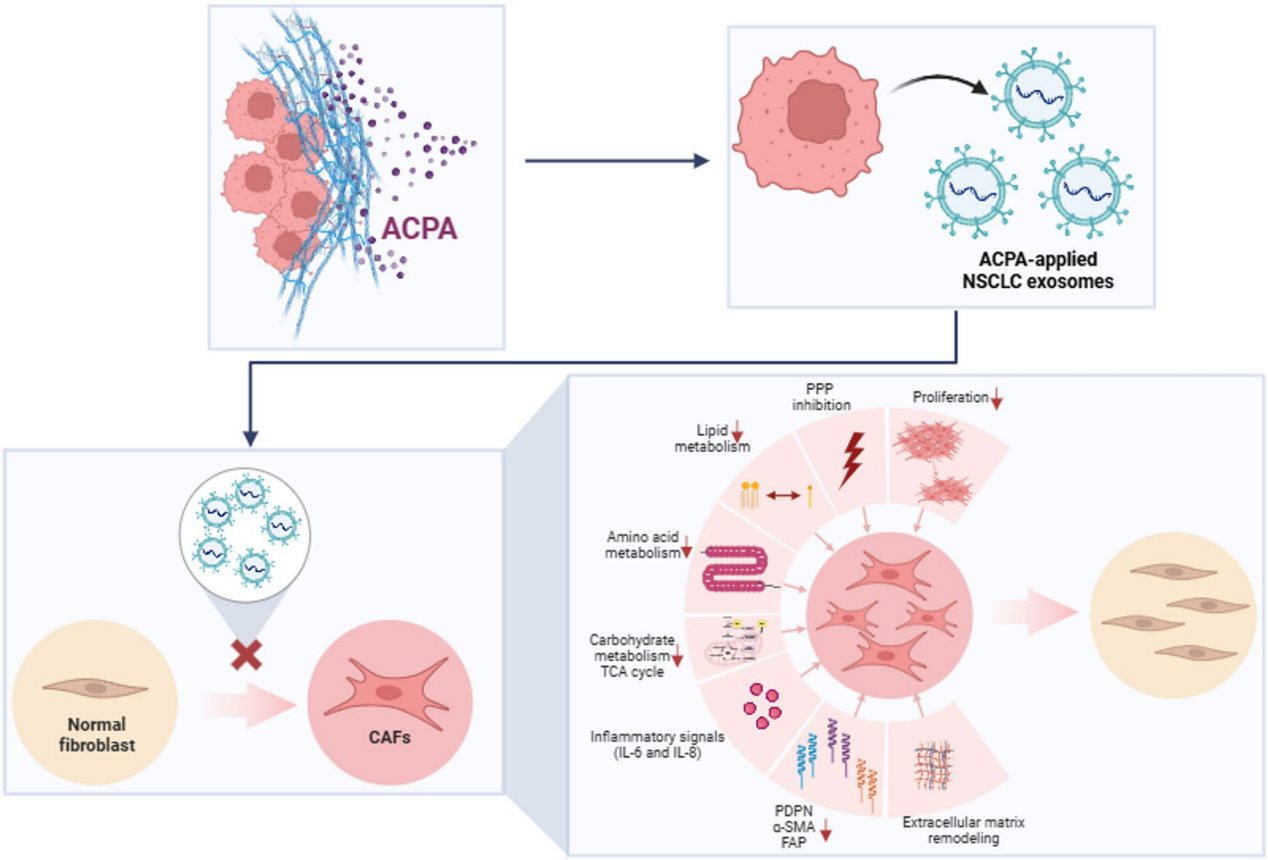


Fig. 5. ACPA reverses normal lung fibroblast transformation to CAFs via NSCLC cell exosome delivery. *Created in*https://BioRender.com.

fully inhibit transformation or cause cytotoxicity in fibroblasts, suggesting mild stress[37]. However, the reduced effect of exosomes at low concentration after the initial 24 h might be due to lysosomal degradation of the internalized exosomes[38,39] or possible upregulation of new pro-fibrotic proteins following the initial stress[40]. Additionally, recipient fibroblasts internalize exosomes through rapid endocytic pathways such as clathrin-mediated endocytosis, caveolin-dependent endocytosis, lipid raft endocytosis, macro-pinocytosis, phagocytosis, or direct membrane fusion[41,42]. This process results in the rapid release of their cargo, such as reduced pro-oncogenic miRNAs like miR-21/23[43], into the cytoplasm, thereby reducing fibroblast activation. The release of pro-oncogenic miRNAs, particularly in exosomes from untreated NSCLC cells (controls), might be sufficient to rapidly trigger the translation of key fibrotic proteins. Here, ACPA exhibited a superior anti-proliferative effect on HLFs compared to co-culture with A549 cells in vitro. Co-culture of NSCLC and HLFs with a ratio of 1:5 presented a better proliferative effect on HLFs when compared to 1:1 and 5:1 A549:LL24 co-culture groups, suggesting the importance of the existence of a greater population of HLFs in the microenvironment. ACPA also diminished PDPN, FAP and α-SMA CAF expressions in the first 24 h compared to control. ACPA when solely applied at lower IC50 (1 pM) previously suppressed NSCLC proliferation and induced apoptosis through CB1 agonism via PI3K/Akt, p38/JNK, Ras/MEK/ERK, glycolysis, citric acid cycle and urea cycle within 24 h in vitro and in vivo[18,19]. ACPA-treated NSCLC cell exosomes at higher doses could be able to suppress the HLF transformation into CAFs. This might be attributed to the higher CB1 receptor expression on tumor cells that enables direct targeting by ACPA or the internalization of a higher amount of exosomes by fibroblasts for an equal anti-tumoral activity of ACPA. NSCLC-derived exosomes significantly increased the activation of WI-38 and IMR90 fibroblasts and α-SMA level via miR-142-3p compared to control[44]. NSCLC exosomes significantly increased the proliferation and α-SMA level of HLF-1 at 72 h compared to control by immunofluorescence[23]. The high PDPN, FAP, and α-SMA markers detected in the control group in our study align with the previous findings[23,44]. Moreover, the CAF transformation capability was suppressed by the potent effect of ACPA. PDPN is known to be raised in CAFs, triggering tumor cell migration and progression[45,46]. FAP and SMA tend to serve as cell surface markers in activated myofibroblasts[46] and predominantly distinguished close to epithelial tumor cells[47] generally correlates with poor survival. We demonstrated, for the first time, that a cannabinoid-mediated effect of NSCLC exosomes act as a barrier to transformation into CAF-like cells.

We demonstrated that ACPA reduced erythrose 4-phosphate, glucose, glucuronic acid, cholesterol, alanine, glycine, isoleucine, norleucine and FAD levels, whereas it promoted mannitol and malonic acid levels in HLFs on day 1. Our metabolomics data highlights the fundamental anti-proliferative pathways of HLFs in the tumor

niche. The reduction in erythrose 4-phosphate and glucose might indicate the impaired energy metabolism and anabolic pathways (pentose phosphate pathway) which might make the fibroblasts susceptible to damage[48,49]. Glucuronic acid has a key role in detoxification and proteoglycan synthesis and its significant decrease in CAFs might impair extracellular matrix maintenance leading to a reduction in the proliferative capacity of the tumor cells[50]. Moreover, the decrease in cholesterol could affect the cell membrane fluidity and survival[51], which might indicate the weakened CAF membrane network. CAFs heavily rely on protein synthesis to reshape TME, contributing to tumor progression[52].

Our metabolomics data revealed changes in lipid metabolism and amino acids like glycine, which are key to ferroptosis. Ferroptosis is a controlled cell death process that manages lipid peroxidation and redox balance through amino acid antiporter systems, affecting both cancer and stromal cells[53]. These metabolic shifts may indicate ferroptotic activation in fibroblasts, likely due to the anti-tumor effects of ACPA-treated NSCLC cell exosomes. Alternatively, the very low amino acid levels in fibroblasts exposed to these exosomes suggest that ACPA may exert anti-proliferative and stress-inducing effects by increasing amino acid breakdown. Decreased FAD levels could also indicate mitochondrial dysfunction and reduced energy production[54,55]. Conversely, higher mannitol levels after ACPA treatment might show an attempt by fibroblasts to combat oxidative stress, while elevated malonic acid could reflect impaired mitochondrial respiration and increased autophagy, as it inhibits succinate dehydrogenase in the Krebs cycle[56]. These metabolic changes, compared with untreated controls, occurred alongside early CAF activation markers, highlighting exosomal signalling's role in metabolic reprogramming and inhibiting fibroblast activation. Overall, ACPA might disrupt key metabolites involved in the pentose phosphate pathway, lipid metabolism, and amino acid pathways.

Herein, ACPA-treated NSCLC exosomes did not alter the IL-6/-8 secretion profile of HLFs at 24–72 h compared to the control. IL-6 is a pleiotropic cytokine that directly influences the induction of the CAF phenotype by promoting α-SMA[57], and IL-8 promotes fibroblast activation and angiogenesis[58]. Given their importance in targeting fibroblasts, IL-6 and -8 are considered promising biomarkers for demonstrating CAF transformation and tumor growth potential. Exosomes derived from Osimertinib-resistant NSCLC cells increased IL-6 and IL-8 mRNA levels in MRC-5 HLFs at 48 h compared to the control[59]. Since IL-6 and IL-8 are vital in acute-phase responses, their levels during early inflammatory stages should be analysed at multiple time points. Conversely, the IL-6 and IL-8 secretion profiles demonstrate transient increases at specific intervals, despite the overall inhibitory effects of ACPA-treated NSCLC cell exosomes on fibroblast activation. The rise in IL-6/IL-8 levels caused by ACPA-treated NSCLC cell exosomes after 24 h may reflect a temporary stress response or an inflammatory reaction following exosome internalization, rather than a tumor-promoting effect, as these cytokines also contribute to remodelling processes[60]. Therefore, the dual functions of these cytokines could be activated concurrently with the anti-fibrotic effect[60,61].

Within the scope of this preliminary study, the profiles of miR-21 and miR-23 in control and ACPA-treated NSCLC cell exosomes, and their influence on fibroblasts, were evaluated solely. However, a functional analysis of these miRNAs in reducing fibroblast proliferation and suppressing secretion profiles remains unexplored and represents a significant limitation of the study. Our study reveals a highly specific correlation that functionally aligns with established literature showing miRNAs whose high expression in lung tumor cell exosomes is already documented[62,63]. We showed that ACPA selectively inhibits the protumorigenic effects mediated by CAFs via NSCLC cell exosomes by reducing the exosomal levels of miR-21 and miR-23 within the TME, which are two of the most well-documented pro-tumorigenic miRNAs. Moreover, the subsequent reversal of CAF markers (α-SMA, FAP) in the fibroblasts provides strong correlative functional evidence that these two miRNAs as potent regulators of CAF activation[64,65], clearly illustrating how the mechanism operates at this stage of the research. Consequently, these findings persist in adding to the literature, providing innovative insights for future research[66,67]. This study lacks direct exosome uptake by lung fibroblasts, which may prevent a definitive distinction between differential uptake kinetics and a true biological response. However, our primary aim was initially to determine the optimal therapeutic concentration that maximally suppresses fibroblast activation without significant cytotoxicity. The slight viability increase at 10 µg/ml, which suggests a genuine hormetic response, was observed but not further examined mechanistically. Additionally, a low dose of exosomes may not be enough to fully inhibit, instead serving as a mild stressor to the fibroblasts[37]. Therefore, we interpret the data for the 10 µg/ml dose as a typical response of fibroblasts to a lower exosome concentration. Our subsequent metabolomic analysis was intentionally limited to one highly effective dose compared to untreated control. This choice aimed to clearly define the metabolic signature linked to the maximum therapeutic effect of ACPA, focusing the mechanistic discussion on the most relevant anti-tumor action. Herein, we did not assess additional cytokines such as IL-33, TGF-β, stromal cell derived factor-1 (SDF-1), and CAF-derived cardiotrophin-like cytokine factor 1 (CLCF1)[68]. Our analysis of IL-6, IL-8, and classical CAF markers including α-SMA, FAP, and PDPN still provides robust evidence for NSCLC exosome-mediated fibroblast activation, supporting the validity of our findings. Our experimental design did not involve direct loading of ACPA into exosomes, however, future proteomic or mass spectrometry-based analyses would be valuable to determine whether ACPA is physically associated with exosomes or acts indirectly by modulating exosome-producing cells. The observed effects on recipient cells still support the functional relevance of exosome-mediated signaling. The output is limited to in vitro conditions. These findings, therefore, require further validation through additional functional ex vivo and in vivo studies. However, a high-impact molecular dataset with a large sample size and a normal distribution outline for the first time, demonstrating the potency of CB agonistic ACPA targeting the TME by CAFs.

Cannabinoids are emerging as promising candidates in oncology, extending their established role in preventing nausea[69]. Various ongoing and completed clinical trials are exploring the benefits of cannabinoids in managing cancer-related symptoms for patients with NSCLC (ClinicalTrials.gov IDs: NCT06418204, NCT02675842, NCT02802540, and NCT04155008). By modulating the TME through CAF interactions, cannabinoids provide a

novel approach to hinder tumor progression. Therefore, this research highlights the realization of the anti-tumor effects of ACPA on CAF transformation, paving the way for their inclusion in clinical phase trials.

In conclusion, ACPA emerges as a potent therapeutic due to its ability to target both the tumor and accessory cells. Furthermore, it could suppress the protumorigenic effects mediated by CAFs via NSCLC cell exosomes, acting as prospective carriers, within the TME. Most CAF-targeted cancer therapies directly act on fibroblastic but tumor cell behaviors (4 ongoing/completed clinical trials; ClinicalTrials.gov IDs NCT06107608, NCT06024538, NCT01976741 and NCT01593995). This brings up the possibility of ACPA as a potential chemotherapeutic not only in NSCLC but also in other solid tumors. As such, ACPA is a promising candidate that warrants further investigation in vivo or ex vivo models, and, subsequently, clinical trials for its potency in modulating tumor cells along with the stromal cells and reprogramming the TME of NSCLC and other respiratory system and solid tumors.

Materials and methods

Cell culture and drug application

A549 non-small cell lung adenocarcinoma cell line A549 (CCL- 185) and LL24 healthy lung fibroblasts (CCL-151) (all from ATCC, USA) were cultured with DMEM High Glucose and Ham's F12K, respectively, supplemented with 10–15% fetal bovine serum (FBS, Capricorn, USA), or 2% L-glutamine (Capricorn, USA) and 1% penicillin-streptomycin (Capricorn, USA). Cells were cultured at 37 °C in an incubator containing 5% CO_2.

IC50 ACPA (1.39×10^{-12} M)[18] in media containing exosome-depleted FBS was applied to A549 cells for 24 h as previously determined.

Exosome purification and characterization

Supernatants obtained from drug-free and drug-treated A549 cells were centrifuged at 10 000 x g for 10 min to remove cells and debris. After centrifugation, the supernatants were filtered through 0.22 µm pore diameter filters, followed by ultracentrifugation at 220 000 x g for 90 min at + 4 °C. After repeating the ultracentrifugation step twice, the resulting pellet was dissolved in PBS and stored in -80 °C refrigerator. A BCA assay kit (#23225, Thermo Scientific, USA) assessed the total protein concentration according to the manufacturer's instructions. Malvern Nano ZS (Malvern Instruments, Ltd., Worcestershire, UK) device measured the PS, PDI and ZP; NTA (Nanosight NS300, Malvern Analytical, UK) detected the particle numbers and particle size dispersity[27]. Exosomes were diluted to 1:100 and 1:1000 and measured at 23.6 °C with a detection threshold of 20 ($n = 3$).

The presence of surface markers CD9, CD63, and CD81 was determined by FCM for further characterization. Briefly, diluted and centrifuged aldehyde/sulfate latex beads (#2198595, Invitrogen, USA) in PBS were incubated at room temperature on a shaker for 30 min, followed by the addition of unconjugated anti-CD9 (#312102, Biolegend) and incubation overnight at 4 °C on a shaker. The samples were centrifuged at 12 000 × g for 10 min, and the pellet was resuspended in 5% BSA and incubated for 2 h. 5 µg of exosome sample was added to the mixture and incubated for an additional 2 h on a shaker. After washing, anti-human CD9-APC (#E-AB-F1086E, Elabscience, USA), anti-human CD63-FITC (#353006, Biolegend, USA), and anti-human CD81-PE (#349506, Biolegend, USA) antibodies were added at a 1:100 dilution and incubated for 2 h at 4 °C on a shaker. The samples were then washed by centrifugation at 12 000 × g for 10 min at 4 °C. Finally, the samples were resuspended in 100 µl of PBS and analyzed using a NovoCyte flow cytometer (ACEA, USA)[27,70].

For the ultrastructural characterization, 5 µl of the exosome samples were dropped onto 100–200 mesh formwar-coated copper grids and kept for 20 min for the exosomes to settle on the grid. The grids were then kept in phosphotungustic acid (PTA, Sigma, Germany) for 10 min and in uranyl acetate (UA, Sigma, Germany) for 15 min and washed with distilled water. The grids were dried by removing excess water from the edges of the grid with filter paper. The exosome diameters were measured under a transmission electron microscope (Jeol, JEM1400, Japan). All characterization studies were performed trice.

Quantitative Real-Time polymerase chain reaction (qRT-PCR)

Gene expression analysis was performed to detect miR-21 and miR-23 expression in exosomes obtained from control and ACPA-treated A549 NSCLC cells as previously done[71]. Briefly, the cell-trizol mixture was centrifuged at 12 000 x g at 4 °C for 10 min. After adding chloroform to the samples, they were centrifuged for 15 min. The mixture was passed through the kit columns (#305 − 101, GeneAll, South Korea) according to manufacturer's instructions, the purified miRNA samples were reconstituted in nuclease-free water and purities and concentrations were determined by NanoDrop spectrophotometer (NanoDrop 1000, ThermoScientific, Massachusetts, USA) at 260–280 nm wavelength. Following cDNA synthesis by using stem-loop reverse transcriptase primers with a reaction series of incubation at 25 °C for 10 min, 37 °C for 120 min, 85 °C for 5 min and 4 °C for 1 h, the cDNAs were mixed with iTAG Universal Sybr Green master mix (#17225124, Biorad), forward and reverse primers, and RNase-free water, followed by qRT-PCR in the CFX Connect instrument (Biorad, California, USA). U6 was used as a housekeeping gene. The Cq values of miRNAs in the ACPA-applied group were compared with those of the control ($n = 4$). The experimental results were calculated with the "$2^{-\Delta\Delta CT}$"[71].

Cell viability by MTT assay

ACPA-treated or control A549 NSCLC exosomes were diluted to 0, 10, 50 and 100 µg/ml in LL24 fibroblast media containing exosome-depleted FBS[72,73]. LL24 cells were seeded in 96-well plates at 1×10^5 cells/well, followed by exosome application ($n = 5$). Absorbances at 24, 48 and 72 h were measured at 590 nm wavelength by VersaMax Microplate Reader (Molecular Device, USA) after adding 0.5 mg/ml MTT solution and incubation for 2 h.

Real-Time proliferation analysis (RTCA)

IC50 of ACPA-treated or control A549 NSCLC exosomes were assessed by xCELLigence (ACEA, Roche Applied System)[18]. LL24 cells were seeded at a concentration of 5×10^3 cells/well in 96-well plates coated with gold microelectrodes enabling the recording of impedance as a "cell index" and once the cell index exceeds 1.0, 10, 50 and 100 µg/ml ACPA-treated or control A549 NSCLC exosomes were applied to cells every 24 h for 3 days (n = 3) and cell indices were compared with control medium- and medium including exosome-depleted FBS-applied cells (n = 6). To fully elucidate the effect of A549 cells on LL24 healthy fibroblasts, A549 cells were seeded on inserts at a ratio of 1:1, 1:5 or 5:1 in 96-well plates (n = 6). ACPA at a dose range of 10^{-9}-10^{-12} M[18] were also applied to LL24 cells to observe the sole effect of ACPA on healthy fibroblasts (n = 6).

Flow cytometry

PDPN, FAP and α-SMA cell surface markers were evaluated for CAF activation in exosome-treated LL24 cells by FCM[74]. 3-5 × 10^5 cells were fixed with 3% paraformaldehyde (PFA) and incubated for 15 min at + 4 °C, then washed twice with PBS and centrifuged at + 4 °C for 5 min at 500 x g. Following the incubation with anti-human FAP (#BMS168, Invitrogen), anti-human α-SMA (#ab150301, Abcam) and anti-human podoplanin (#ab10288, Abcam)[75,76] primary antibodies in 1% bovine serum albumin (BSA) and 0.1% sodium azide/PBS for 1 h at + 4 °C, the cells were washed and incubated with IgG secondary antibody (#ab7086, Abcam) in the dark for 30 min. After washing, the resulting cell pellet was resuspended in PBS and analyzed on a flow cytometry device (Novocyte 2000R Flow Cytometer System, Agilent, USA) (n = 3).

ELISA

The IL-6 (#D6050, R&D Systems) and IL-8 (#D8000C, R&D Systems) secretome profile of NSCLC exosome-treated CAFs was evaluated by ELISA. The supernatants were collected, centrifuged at 12,000 rpm for 5 min and the labeling was carried out according to the instructions. The absorbances were measured at 450 nm wavelength in a microplate reader (n = 3).

Metabolomics analysis

Metabolomic profiling of 100 µg/ml control and 50 µg/ml ACPA-applied A549 cell exosomes-administered LL24 cells for 12 h was conducted as previously reported[18,77]. Briefly, following the administration, LL24 cells were extracted using methanol: water mixture (9:1, v/v) and analyzed using total ion count (TIC) normalization by GC-MS after methoxyamination and derivatization (n = 3).

Statistical analysis

All data followed normal distribution per Shapiro-Wilk test. Independent t-test compared control and ACPA-treated NSCLC exosome miRNA levels by qRT-PCR. MTT, proliferation, metabolomics and ELISA data were analyzed with one-way ANOVA and post-hoc Duncan's test. Results are shown as mean ± SD, evaluated within 95% CI. All statistical analyses were performed using SPSS v25 and Graphpad Prism 8.

Data availability

All data generated or analysed during this study are included in this article.

Received: 25 September 2025; Accepted: 19 November 2025
Published online: 28 November 2025

References

1. Bray, F. et al. Global cancer statistics 2022: GLOBOCAN estimates of incidence and mortality worldwide for 36 cancers in 185 countries. *Cancer J. Clin.* **74**, 229–263 (2024).
2. Guo, Q. et al. Current treatments for non-small cell lung cancer. *Front. Oncol.* **12**, 945102 (2022).
3. Myers, D. J. & Wallen, J. M. in *StatPearls* (StatPearls Publishing Copyright © 2025, StatPearls Publishing LLC., (2025).
4. Kim, C. S. & Jeter, M. D. in *StatPearls* (StatPearls Publishing Copyright © 2022, StatPearls Publishing LLC., (2022).
5. Lin, X. et al. Regulatory mechanisms of PD-1/PD-L1 in cancers. *Mol. Cancer.* **23**, 108 (2024).
6. Qiu, J. et al. Immunomodulatory precision: A narrative review exploring the critical role of immune checkpoint inhibitors in cancer treatment. *Int. J. Mol. Sci.* **25**, 5490 (2024).
7. Boyacıoğlu, Ö. & Korkusuz, P. in *Cell Biology and Translational Medicine, Volume 19: Perspectives in Diverse Human Diseases and Their Therapeutic Options* (ed Kursad Turksen) 145–169Springer Nature Switzerland, (2023).
8. Boyacıoğlu, Ö., Kalali, B. D., Tongün, E. & Korkusuz P. 1–27 (Springer International Publishing, (2025).
9. Irvine, A. F., Waise, S., Green, E. W., Stuart, B. & Thomas, G. J. Characterising cancer-associated fibroblast heterogeneity in non-small cell lung cancer: a systematic review and meta-analysis. *Sci. Rep.* **11**, 3727 (2021).
10. Zhang, H. et al. Define cancer-associated fibroblasts (CAFs) in the tumor microenvironment: new opportunities in cancer immunotherapy and advances in clinical trials. *Mol. Cancer.* **22**, 159 (2023).
11. Czekay, R. P., Cheon, D. J., Samarakoon, R., Kutz, S. M. & Higgins, P. J. Cancer-Associated fibroblasts: mechanisms of tumor progression and novel therapeutic targets. *Cancers (Basel).* **14**, 1231 (2022).
12. Feng, Y. et al. Targeting CAFs and extracellular matrix (ECM) in lung cancer: potential of adjuvants and nanoparticles. *Bioorg. Chem.* **162**, 108586 (2025).
13. Tokhanbigli, S., Haghi, M., Dua, K. & Oliver, B. G. G. Cancer-associated fibroblast cell surface markers as potential biomarkers or therapeutic targets in lung cancer. *Cancer Drug Resist.* **7**, 32 (2024).
14. Wang, X. et al. Overcoming cancer treatment resistance: unraveling the role of cancer-associated fibroblasts. *J. Natl. Cancer Cent.* **5**, 237–251 (2025).
15. Wu, F. et al. Signaling pathways in cancer-associated fibroblasts and targeted therapy for cancer. *Signal. Transduct. Target. Ther.* **6**, 218 (2021).
16. Giusti, I. et al. Tumor-Derived extracellular vesicles activate normal human fibroblasts to a Cancer-Associated Fibroblast-Like Phenotype, sustaining a Pro-Tumorigenic microenvironment. *Front. Oncol.* **12**, 839880 (2022).

17. Tomko, A. M., Whynot, E. G., Ellis, L. D. & Dupré, D. J. Anti-cancer potential of cannabinoids, terpenes, and flavonoids present in cannabis. *Cancers (Basel)* **12**, 7 (2020).
18. Boyacıoğlu, Ö. et al. ACPA decreases non-small cell lung cancer line growth through Akt/PI3K and JNK pathways in vitro. *Cell. Death Dis.* **12**, 56 (2021).
19. Boyacıoğlu, Ö. et al. A novel injectable nanotherapeutic platform increasing the bioavailability and anti-tumor efficacy of Arachidonylcyclopropylamide on an ectopic non-small cell lung cancer xenograft model: A randomized controlled trial. *Int. J. Pharm.* **670**, 125153 (2025).
20. Boyacioglu, O. et al. *U S Patent Application No* 17/617,008. (Google Patents US20220168245A1) (2022).
21. Bilgic, E. et al. Endocannabinoids modulate apoptosis in endometriosis and adenomyosis. *Acta Histochem.* **119**, 523–532 (2017).
22. Zorba, B. I. et al. CB65 and novel CB65 liposomal system suppress MG63 and Saos-2 osteosarcoma cell growth in vitro. *J. Liposome Res.* **34**, 274–287 (2024).
23. Huang, J., Ding, Z. P., Luo, Q. Q. & Xu, W. R. Cancer cell-derived exosomes promote cell proliferation and inhibit cell apoptosis of both normal lung fibroblasts and non-small cell lung cancer cell through delivering alpha-smooth muscle actin. *Am. J. Translational Res.* **11**, 1711– (2019).
24. Tajik, T., Baghaei, K., Moghadam, V. E., Farrokhi, N. & Salami, S. A. Extracellular vesicles of cannabis with high CBD content induce anticancer signaling in human hepatocellular carcinoma. *Biomed. Pharmacother.* **152**, 113209 (2022).
25. Kosgodage, U. S. et al. Cannabidiol affects extracellular vesicle Release, miR21 and miR126, and reduces prohibitin protein in glioblastoma multiforme calls. *Translational Oncol.* **12**, 513–522 (2019).
26. Boyacioglu, O. et al. 58P novel NanoACPA delivery system presents antitumor effect on ectopic non-small cell lung cancer xenograft model. *ESMO Open* **9**, 102287 (2024).
27. Ciftci, E. et al. Comparative analysis of magnetically activated cell sorting and ultracentrifugation methods for exosome isolation. *PLOS ONE*. **18**, e0282238 (2023).
28. Wang, Y. et al. Docetaxel-loaded exosomes for targeting non-small cell lung cancer: Preparation and evaluation in vitro and in vivo. *Drug Deliv*. **28**, 1510–1523 (2021).
29. Mashouri, L. et al. Exosomes: composition, biogenesis, and mechanisms in cancer metastasis and drug resistance. *Mol. Cancer*. **18**, 75 (2019).
30. Kim, H. I. et al. Recent advances in extracellular vesicles for therapeutic cargo delivery. *Exp. Mol. Med.* **56**, 836–849 (2024).
31. Signorelli, D. et al. Circulating CD81-expressing extracellular vesicles as biomarkers of response for immune-checkpoint inhibitors in advanced NSCLC. *Front. Immunol.* **13**, 987639 (2022).
32. Fan, J., Xu, G., Chang, Z., Zhu, L. & Yao, J. miR-210 transferred by lung cancer cell derived exosomes May act as proangiogenic factor in cancer-associated fibroblasts by modulating JAK2/STAT3 pathway. *Clin. Sci.* **134**, 807–825 (2020).
33. Jin, J. & Yu, G. Hypoxic lung cancer cell-derived Exosomal miR-21 mediates macrophage M2 polarization and promotes cancer cell proliferation through targeting IRF1. *World J. Surg. Oncol.* **20**, 241 (2022).
34. Duréndez-Sáez, E. et al. Exosomal MicroRNAs in non-small cell lung cancer. *Transl Cancer Res.* **10**, 3128–3139 (2021).
35. Hsu, Y. L. et al. Hypoxic lung cancer-secreted Exosomal miR-23a increased angiogenesis and vascular permeability by targeting Prolyl hydroxylase and tight junction protein ZO-1. *Oncogene* **36**, 4929–4942 (2017).
36. Leri, M. et al. Healthy effects of plant polyphenols: molecular mechanisms. *Int. J. Mol. Sci.* **21**, 1250 (2020).
37. Hagey, D. W. et al. The cellular response to extracellular vesicles is dependent on their cell source and dose. *Sci. Adv.* **9**, eadh1168 (2023).
38. Gurung, S., Perocheau, D., Touramanidou, L. & Baruteau, J. The exosome journey: from biogenesis to uptake and intracellular signalling. *Cell. Communication Signal.* **19**, 47 (2021).
39. Wei, H. et al. Regulation of exosome production and cargo sorting. *Int. J. Biol. Sci.* **17**, 163–177 (2021).
40. Zhang, M. et al. Exosomes from senescent epithelial cells activate pulmonary fibroblasts via the miR-217-5p/Sirt1 axis in paraquat-induced pulmonary fibrosis. *J. Translational Med.* **22**, 310 (2024).
41. Wang, Y., Xiao, T., Zhao, C. & Li, G. The regulation of exosome generation and function in physiological and pathological processes. *Int. J. Mol. Sci.* **25**, 255 (2024).
42. Gonda, A., Moyron, R., Kabagwira, J. Vallejos, P. & Wall, N. R. Cellular-Defined Microenvironmental Internalization of Exosomes in *Extracellular Vesicles and their Importance in Human Health* (eds Ana Gil De Bona & Jose Antonio Reales-Calderon) (IntechOpen, 2019).
43. Lau, N. C. H. & Yam, J. W. P. From exosome biogenesis to absorption: key takeaways for cancer research. *Cancers (Basel)* **15**, 7 (2023).
44. Lawson, J. et al. Extracellular vesicle secretion of miR-142-3p from lung adenocarcinoma cells induces tumor promoting changes in the stroma through cell-cell communication. *Mol. Carcinog.* **58**, 376–387 (2019).
45. Suzuki, J. et al. Relationship between podoplanin-expressing cancer-associated fibroblasts and the immune microenvironment of early lung squamous cell carcinoma. *Lung Cancer*. **153**, 1–10 (2021).
46. Mhaidly, R. & Mechta-Grigoriou, F. Fibroblast heterogeneity in tumor micro-environment: role in immunosuppression and new therapies. *Semin. Immunol.* **48**, 101417 (2020).
47. Linares, J., Marín-Jiménez, J. A., Badia-Ramentol, J. & Calon, A. Determinants and functions of CAFs secretome during cancer progression and therapy. *Front. Cell. Dev. Biol.* **8**, 621070 (2021).
48. TeSlaa, T., Ralser, M., Fan, J. & Rabinowitz, J. D. The Pentose phosphate pathway in health and disease. *Nat. Metab.* **5**, 1275–1289 (2023).
49. Li, J. et al. Metabolic reprogramming of pulmonary fibrosis. *Front. Pharmacol.* **13**, 1031890 (2022).
50. Gao, Q. et al. Dysregulated glucuronic acid metabolism exacerbates hepatocellular carcinoma progression and metastasis through the TGFβ signalling pathway. *Clin. Transl Med.* **12**, e995 (2022).
51. Paukner, K., Králová Lesná, I. & Poledne, R. Cholesterol in the cell Membrane-An emerging player in atherogenesis. *Int J. Mol. Sci.* **23**, 533 (2022).
52. Chen, Y., Zhang, X., Yang, H., Liang, T. & Bai, X. The Self-eating of cancer-associated fibroblast: A potential target for cancer. *Biomed. Pharmacother.* **163**, 114762 (2023).
53. Ebrahimnezhad, M., Valizadeh, A. & Yousefi, B. Ferroptosis and immunotherapy: breaking barriers in cancer treatment resistance. *Crit. Rev. Oncol. Hematol.* **214**, 104907 (2025).
54. Orooji, N., Fadaee, M., Kazemi, T. & Yousefi, B. Exosome therapeutics for non-small cell lung cancer tumorigenesis. *Cancer Cell Int.* **24**, 360 (2024).
55. Casanova, A., Wevers, A., Navarro-Ledesma, S. & Pruimboom, L. Mitochondria: It is all about energy. *Front Physiol* 14, 1114231 (2023).
56. Cui, H. et al. Malonate differentially affects cell survival and confers chemoresistance in cancer cells via the induction of p53-dependent autophagy. *Biochem. Pharmacol.* **219**, 115950 (2024).
57. Liu, X., Wang, C., Mao, H. & Wei, J. Crosstalk between cancer–associated fibroblasts and inflammation in tumor microenvironment: A novel perspective in cancer therapy (Review). *Oncol. Rep.* **54**, 93 (2025).
58. GEINDREAU, M., BRUCHARD, M. & VEGRAN, F. Role of cytokines and chemokines in angiogenesis in a tumor context. *Cancers (Basel)*. **14**, 2446 (2022).
59. Song, L., Qian, G., Huang, J., Chen, T. & Yang, Y. AZD9291-resistant non-small cell lung cancer cell-derived Exosomal lnc-MZT2A-5:1 induces the activation of fibroblasts. *Ann. Transl Med.* **9**, 1593 (2021).

60. Huang, S. et al. Exosomes in inflammation and cancer: from bench to bedside applications. *Mol. Biomed.* **6**, 41 (2025).
61. Jing, F. et al. An herbal product alleviates Bleomycin-Induced pulmonary fibrosis in mice via regulating NF-κB/TNF-α signaling in macrophages. *Front. Pharmacol.* **13**, 805432 (2022).
62. Hussain, S. et al. MicroRNAs modulation in lung cancer: exploring dual mechanisms and clinical prospects. *BIOCELL* **48**, 403–413 (2024).
63. Wang, J. et al. Research advances of extracellular vesicles in lung diseases. *Cell Transplant.* **34**, 09636897251362031 (2025).
64. Kunita, A. et al. MicroRNA-21 in cancer-associated fibroblasts supports lung adenocarcinoma progression. *Sci. Rep.* **8**, 8838 (2018).
65. Song, Y., Kelava, L. & Kiss, I. MiRNAs in lung adenocarcinoma: Role, Diagnosis, Prognosis, and therapy. *Int. J. Mol. Sci.* **24**, 13302 (2023).
66. Hetta, H. F. et al. Circulating miRNA-21 and miRNA-23a expression signature as potential biomarkers for early detection of Non-Small-Cell lung cancer. *Microrna* **8**, 206–215 (2019).
67. Luo, H. et al. The miR-23a/27a/24 – 2 cluster drives immune evasion and resistance to PD-1/PD-L1 Blockade in non-small cell lung cancer. *Mol. Cancer*. **23**, 285 (2024).
68. Peng, Z., Tong, Z., Ren, Z., Ye, M. & Hu, K. Cancer-associated fibroblasts and its derived exosomes: a new perspective for reshaping the tumor microenvironment. *Mol. Med.* **29**, 66 (2023).
69. Bathula, P. P. & Maciver, M. B. Cannabinoids in treating Chemotherapy-Induced nausea and Vomiting, Cancer-Associated Pain, and tumor growth. *Int. J. Mol. Sci.* **25**, 74 (2024).
70. Çam, S. B., Çiftci, E., Gürbüz, N., Altun, B. & Korkusuz, P. Allogeneic bone marrow mesenchymal stem cell-derived exosomes alleviate human hypoxic AKI-on-a-Chip within a tight treatment window. *Stem Cell. Res. Ther.* **15**, 105 (2024).
71. Kılıç, N. et al. Thioredoxin System and miR-21, miR-23a/b and let-7a as Potential Biomarkers for Brain Tumor Progression: Preliminary Case Data. *World Neurosurgery* (2022).
72. Wang, L. et al. Lung CSC-derived Exosomal miR-210-3p contributes to a pro-metastatic phenotype in lung cancer by targeting FGFRL1. *J. Cell. Mol. Med.* **24**, 6324–6339 (2020).
73. Sun, L. et al. Clodronate-loaded liposomal and fibroblast-derived Exosomal hybrid system for enhanced drug delivery to pulmonary fibrosis. *Biomaterials* **271**, 120761 (2021).
74. Nurmik, M., Ullmann, P., Rodriguez, F., Haan, S. & Letellier, E. In search of definitions: Cancer-associated fibroblasts and their markers. *Int. J. Cancer*. **146**, 895–905 (2020).
75. Katsube, R. et al. Fibroblast activation protein targeted near infrared photoimmunotherapy (NIR PIT) overcomes therapeutic resistance in human esophageal cancer. *Sci. Rep.* **11**, 1693 (2021).
76. Łabędź, N. et al. Modulation of Fibroblast Activity via Vitamin D3 Is Dependent on Tumor Type—Studies on Mouse Mammary Gland Cancer. *Cancers (Basel)* 14, 4585 (2022).
77. Boyacıoğlu, Ö., Reçber, T., Kır, S., Korkusuz, P. & Nemutlu, E. Development and validation of a sensitive assay for the quantification of Arachidonoylcyclopropylamide (ACPA) in cell culture by LC–MS/MS. *J. Anal. Sci. Technol.* **14**, 18 (2023).

Acknowledgements
We kindly acknowledge Beliz Taskonak for her technical assistance with MTT and ELISA assays. We also kindly acknowledge Merve Gizer, Ph.D. for her technical assistance with TEM characterization experiments.

Author contributions
ÖB designed and performed the experiments, analyzed and interpreted data and wrote the manuscript. BDK contributed to the design and performed the experiments. EN and TR contributed to the metabolomics analysis of LL24 fibroblasts. İE and DGG performed zeta sizer measurements, edited the paper and provided feedback. NK contributed to qRT-PCR analysis, edited the paper and provided feedback. PK conceived the project, supervised the research and wrote and edited the paper. All authors wrote and reviewed the final version of the manuscript.

Funding
This study was supported by Hacettepe University Scientific Research Projects Coordination Unit (TSA-2023-20427).

Declarations

Competing interests
The authors declare no competing interests.

Ethics approval
None.

Additional information
Correspondence and requests for materials should be addressed to P.K.

Reprints and permissions information is available at www.nature.com/reprints.

Publisher's note Springer Nature remains neutral with regard to jurisdictional claims in published maps and institutional affiliations.

Open Access This article is licensed under a Creative Commons Attribution-NonCommercial-NoDerivatives 4.0 International License, which permits any non-commercial use, sharing, distribution and reproduction in any medium or format, as long as you give appropriate credit to the original author(s) and the source, provide a link to the Creative Commons licence, and indicate if you modified the licensed material. You do not have permission under this licence to share adapted material derived from this article or parts of it. The images or other third party material in this article are included in the article's Creative Commons licence, unless indicated otherwise in a credit line to the material. If material is not included in the article's Creative Commons licence and your intended use is not permitted by statutory regulation or exceeds the permitted use, you will need to obtain permission directly from the copyright holder. To view a copy of this licence, visit http://creativecommons.org/licenses/by-nc-nd/4.0/.

© The Author(s) 2025

GCRIS